

# AH-GS: Augmented 3D Gaussian Splatting for High-Frequency Detail Representation

Chenyang Xu<sup>1</sup> XingGuo Deng<sup>1</sup> Rui Zhong<sup>2</sup>  
<sup>1</sup>Fuzhou University, <sup>2</sup>Central China Normal University

**Abstract**—The 3D Gaussian Splatting (3D-GS) is a novel method for scene representation and view synthesis. Although Scaffold-GS achieves higher quality real-time rendering compared to the original 3D-GS, its fine-grained rendering of the scene is extremely dependent on adequate viewing angles. The spectral bias of neural network learning results in Scaffold-GS’s poor ability to perceive and learn high-frequency information in the scene. In this work, we propose enhancing the manifold complexity of input features and using network-based feature map loss to improve the image reconstruction quality of 3D-GS models. We introduce AH-GS, which enables 3D Gaussians in structurally complex regions to obtain higher-frequency encodings, allowing the model to more effectively learn the high-frequency information of the scene. Additionally, we incorporate high-frequency reinforce loss to further enhance the model’s ability to capture detailed frequency information. Our result demonstrates that our model significantly improves rendering fidelity, and in specific scenarios (e.g., MipNeRF360-garden), our method exceeds the rendering quality of Scaffold-GS in just 15K iterations.

**Index Terms**—3D Gaussian Splatting, 3D Reconstruction, Novel View Synthesis, Image-based Rendering

## I. INTRODUCTION

The 3D Gaussian Splatting [1] uses a set of scaled 3D Gaussian primitives to represent the scene. Depending on the given view point, these primitives are projected onto a 2D plane, and the  $\alpha$ -blending is then applied to calculate the pixel colors. While 3D-GS rendered images look realistic, a closer look reveals that the images are often too smooth in detail rendering. To address these limitations, Scaffold-GS [2] introduces anchors to control the distribution of 3D Gaussians and employs MLPs to predict their attributes. This method more effectively distributes the 3D Gaussians according to the scene’s geometry, which alleviates the above problems to some extent. However, as shown in Fig. 1, in challenging areas (eg., texture-less, fine-scale details, light reflections), the rendered images still lose high-frequency details.

The problems mentioned above stem from two fundamental issues. Firstly, due to the limitation of low-dimensional viewing direction, both 3D-GS and Scaffold-GS struggle to capture high-frequency information about the scene. Scaffold-GS uses a three-dimensional viewing direction as input and employs individual MLPs to predict the attributes of 3D Gaussians. This approach focuses on the low-frequency information of the scene, allowing it to quickly capture the overall structure. However, because low-frequency viewing directions lack high-frequency components, the model’s ability to explore finer details is limited. Second, pixel loss often does not reflect

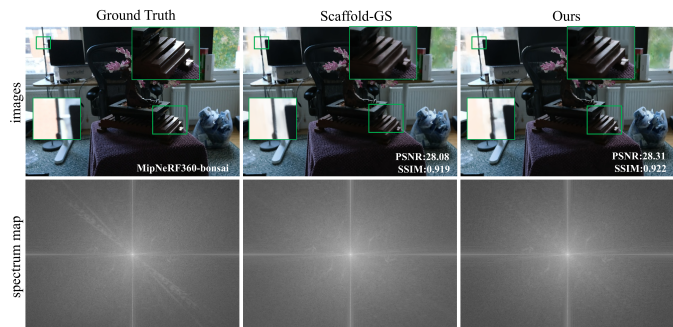


Fig. 1. The spectrum maps rendered by Scaffold-GS [2] lack high-frequency regions, resulting in missing texture details and lighting in the rendered image. In contrast, our method utilizes the structural properties of the scene to better capture high-frequency information, achieving higher quality rendering.

the small differences between the reconstructed image and the real image directly. Pixel loss and structural similarity are commonly used as loss functions for 3D-GS and its enhancement models. However, pixel loss functions mainly focus on the differences in overall pixel values, ignoring high-frequency details and texture information in the image. Additionally, pixel loss functions cannot effectively measure the image quality perceived by the human visual system, resulting in a reconstructed image that may be visually significantly different from the real image.

Our key insight is that enhancing the manifold complexity of viewing features, based on the geometry of the scene, makes it easier to learn the high-frequency components in 3D Gaussian attributes. We proposed AH-GS, which estimates the probability density of local 3D Gaussians and uses this probability distribution as the input to MLPs instead of the traditional viewing direction. Specifically, our model is based on Scaffold-GS, which improves the neural Gaussian derived from the anchor points. Intuitively, we discover that higher Gaussian point density correlates with more complex geometric structures in the scene, which contain higher frequency information. We introduce the Adaptive Frequency Encoding Module (AFEM). First, the viewing direction is encoded using a sinusoidal function, replacing the three-dimensional viewing direction as input to MLPs for predicting the opacity, quaternion, and scaling of 3D Gaussians. Next, based on the Gaussian density of the anchor points, the von Mises-Fisher (vMF) distribution of the viewing direction is calculated. The encoded results and a local context feature are then input

to the color MLP to predict the color of the 3D Gaussian from various viewpoints. Furthermore, we introduce a high-frequency reinforce loss to enhance our model’s ability to learn the scene’s frequency information. In summary, we make the following contributions.

- We present an Adaptive Frequency Encoding Module (AFEM) that enhances direction features based on the structural complexity of the scene. This improvement boosts the 3D-GS-based model’s ability to learn and process high-frequency information within the scene.
- We add a high-frequency reinforce loss in training to better retain the high-frequency details of the scene with less additional training overhead.
- Our method makes some simple modifications based on the Scaffold-GS code, which can also be applied to other 3D-GS models.

## II. RELATED WORK

### A. Novel View Synthesis

Novel View Synthesis (NVS) is a computer vision task aimed at generating new views of an input scene from different camera positions, which has a wide range of applications in the fields of digital twins [3], [4], medical diagnosis [5], [6], and wireless communications [7], [8]. Neural Radiance Field (NeRF) [9] learns a volumetric representation through an MLP to implicitly represent the 3D scene, which can be rendered to obtain a highly realistic scene. However, training NeRF typically requires 100k-300k iterations and involves extensive neural network operations, which limits its applicability in real-time tasks and for high-resolution scenes. Recently, 3D-GS [1] has emerged as an attractive alternative. 3D-GS is a volume rendering technique that represents 3D scenes using 3D Gaussian primitives. Subsequent improvements focus on anti-aliasing [10]–[12], model compression [13], [14], and extending application scenes [8], [15], [16], thereby improving the application of 3D-GS in real large-scale environments. However, both 3D-GS and its improved models predict the color of 3D Gaussians based solely on the viewing direction, neglecting the underlying geometric structure of the scene. In this paper, we propose a novel approach to predict the colors of 3D Gaussian at different locations, accounting for the geometric structure of the scene. We also introduce a high-frequency reinforce loss, designed to better render high-frequency details in the scene and improve the overall image quality.

### B. The Spectral Bias of Deep Learning

Neural networks exhibit a tendency to learn frequencies. Rahaman et al. [17] refer to this phenomenon as spectral bias, suggesting that neural networks tend to learn components of lower complexity more quickly. The research also indicates that the geometry of the data (e.g., dimension) influences the learning of frequency information by neural networks, with complex structures potentially facilitating the learning of high-frequency information. The following work explains spectral bias through information theory [18] and neural cut kernel

functions [19]. Notably, NeRF proposes positional encoding, which maps 3D coordinates to more complex manifold functions, enhancing the model’s ability to capture high-frequency details. We aim to apply a similar approach in Scaffold-GS by increasing the manifold complexity of viewing direction, thereby enabling more efficient learning of high-frequency components in 3D Gaussian attributes.

## III. METHOD

### A. Preliminary

The core of Scaffold-GS is to voxelize the scene and use MLP to dynamically predict the attributes of the  $k$  3D Gaussians controlled by each anchor point  $v$ . Initially, the entire scene is voxelized based on a sparse point cloud generated by COLMAP [20]. The center of each voxel  $\mathbf{V}$  is treated as an anchor point  $v$  with local context features  $\hat{f}_v \in \mathbb{R}^{32}$ , scaling factors  $l_v \in \mathbb{R}^3$ , and  $k$  learnable offsets  $\mathbf{O}_v \in \mathbb{R}^{k \times 3}$ .

Next, anchor points that are not visible within the view are filtered out. The anchor generates the attributes of the  $k$  neural Gaussians it controls. Specifically, the position of  $k$  3D Gaussians is calculated based on the position  $\mathbf{x}$ ,  $k$  learnable offsets  $\{\mathcal{O}_0, \dots, \mathcal{O}_{k-1}\}$ , and scaling factor  $l_v$ .

$$\{\mu_0, \dots, \mu_{k-1}\} = \mathbf{x}_v + \{\mathcal{O}_0, \dots, \mathcal{O}_{k-1}\} \cdot l_v, \quad (1)$$

The viewing direction  $\vec{\mathbf{d}}_{v_c}$ , relative distance  $\delta_{v_c}$  as inputs, and a local context feature  $\hat{f}_v$  are used as inputs to generate  $k$  3D Gaussian attributes, including opacity  $\alpha \in \mathbb{R}$ , covariance-related quaternion  $q \in \mathbb{R}^4$ , scaling  $s \in \mathbb{R}^3$ , and color  $c \in \mathbb{R}^3$ , through independent MLPS ( $F_\alpha, F_c, F_q, F_s$ ).

Afterwards, the 3D scene is treated as a set of scaled 3D Gaussian primitives, and  $\Sigma$  is formulated using a scaling matrix  $S$  and rotation matrix  $R$  to maintain its positive semi-definite property.

$$G(x) = e^{-\frac{1}{2}(x-\mu)^T \Sigma^{-1}(x-\mu)}, \Sigma = R S S^T R^T, \quad (2)$$

The next steps are the same as for 3D-GS, 3D Gaussians are projected onto the 2D screen using the projection formula [21]. Finally, the color of each pixel is rendered via  $\alpha$  blending according to the primitive’s depth order  $1, \dots, K$ .

$$C(x') = \sum_{i \in K} c_i \sigma_i \prod_{j=1}^{k-1} (1 - \sigma_j), \quad \sigma_i = \alpha_i G'_i(x'), \quad (3)$$

The whole rendering process employs a tile-based rasterizer, significantly enhancing rendering speed. Additionally, Scaffold-GS has developed growth and pruning strategies to optimize anchor point distributions.

### B. Adaptive Frequency Encoding Module

The 3D-GS establishes the relationship between viewing angles and 3D Gaussian colors by fitting various training views. However, its capability for color representation from 3D perspectives is limited, and the learned attributes of 3D Gaussians lack high-frequency information. Our key idea is to enhance 3D-GS’s ability to learn high-frequency information by leveraging the distributional characteristics of the scene.

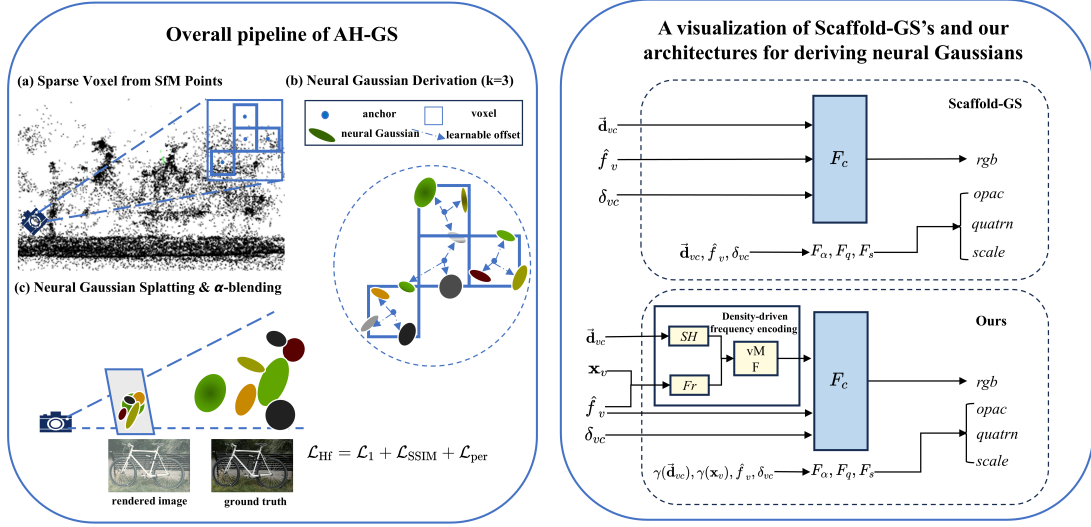


Fig. 2. **Overview of AH-GS.** The left figure illustrates the overall flowchart: first, the scene is voxelized according to the SfM-derived points; then, each anchor point generates the attributes of the neural Gaussians (equivalent to 3D Gaussians) it controls; and finally, neural Gaussians are projected onto a 2D screen, with each pixel rendered using a  $\alpha$ -blending formula. The right figure visually compares our architecture with that of Scaffold-GS. Our model incorporates an Adaptive Frequency Encoding Module, allowing the neural Gaussians in regions of higher structural complexity to accommodate higher frequency variations and better respond to rapid changes in appearance.

*a) Positional encoding:* Positional encoding is a technique that converts raw low-dimensional spatial positions into high-dimensional vector representations. We encode the viewing direction  $\vec{d}_{vc}$  and anchor position  $\mathbf{x}_v$  as inputs to  $F_\alpha$ ,  $F_q$ , and  $F_s$  to predict the  $\alpha \in \mathbb{R}$ ,  $q \in \mathbb{R}^4$ , and  $s \in \mathbb{R}^3$  of the neural Gaussians. For example, the opacity  $\{\alpha_i\}$  of a neural Gaussian derived from an anchor point is given by:

$$\{\alpha_0, \dots, \alpha_{k-1}\} = F_\alpha(\hat{f}_v, \delta_{vc}, \gamma(\vec{d}_{vc}), \gamma(\mathbf{x}_v)), \quad (4)$$

where the function  $\gamma(p)$  is a sinusoidal function, following the same formula as in the NeRF paper [9]. The covariance-related quaternion  $\{q_i\}$  and scaling  $\{s_i\}$  are predicted in a similar way.

*b) Density-driven frequency encoding.:* According to the  $\alpha$ -blending formula, the pixel values of an image are determined by the opacity and color of the 3D Gaussians projected onto the area. We find that the local detail complexity of the scene is directly proportional to the density of the 3D Gaussian at that location. Therefore, we introduce the vMF distribution to represent the structural characteristics of the scene and adjust the code rate of the 3D Gaussian accordingly. The formula for the vMF distribution is as follows:

$$f_p(x; \mu, \kappa) = \frac{1}{C_p(\kappa)} \exp(\kappa \mu^T x) \quad (5)$$

where  $C_p(\kappa)$  is the normalization constant, derived from the first type of modified Bessel function. The mean direction vector is denoted by  $\mu$ , and  $\kappa$  represents the concentration parameter. As  $\kappa$  increases, the distribution becomes more concentrated around  $\mu$ . Conversely, as  $\kappa$  decreases, the distribution becomes more dispersed.

For the voxelized scene, we initially use an MLP  $F_r$  to predict the concentration of neural Gaussians as:

$$\kappa = F_r(\hat{f}_v, \mathbf{x}_v) \quad (6)$$

where  $\mathbf{x}_v$  and  $\hat{f}_v$  denote the anchor position and a local context feature, respectively. Since the  $\kappa$  is independent of  $\vec{d}_{vc}$ , which is not used as an input to  $F_r$ . Subsequently, we establish the link between  $\vec{d}_{vc}$  and  $\kappa$ . Based on the definition of the vMF distribution, we map the  $\vec{d}_{vc}$  onto the unit sphere using a spherical harmonic. To enable better frequency representation, we use the a set of spherical harmonic  $Y_\ell^m$ .

$$Y_\ell^m(\vec{d}_{vc}) : (\ell, m) \in \mathcal{M}_L \quad (7)$$

$$\mathcal{M}_L = \{(\ell, m) : \ell = 1, \dots, 2L, m = 0, \dots, \ell\}$$

Finally, the expected value of a spherical harmonic under a vMF distribution is computed and used as input to  $F_c$  to predict the color of neural Gaussians. In our implementation, we utilize the proof from the Ref-NeRF paper [22], which shows that above expectation simplifies to an exponential function multiplied by a spherical harmonic.

$$\begin{aligned} \text{DDFE}(\vec{d}_{vc}, \kappa) &= \mathbb{E}_{\vec{d}_{vc} \sim \text{vMF}(\vec{d}_{vc}, \kappa)} [Y_\ell^m(\vec{d}_{vc})] \\ &= A_\ell(\kappa) Y_\ell^m(\vec{d}_{vc}) \end{aligned} \quad (8)$$

Although our approach is similar to the integrated directional encoding in Ref-NeRF, their underlying principles are distinct. We use Density-driven frequency encoding to encode directions at higher Gaussian point density locations with higher code rates to capture more scene details. Conversely, in areas with low Gaussian density, directions are encoded

at a lower frequency and rendered in flatter colors. The integrated direction encoding is based on allowing smooth areas to receive higher frequency reflection direction encoding, depending on the material’s roughness.

### C. High-frequency reinforce loss

$\mathcal{L}_1$  loss is commonly used to supervise the training of 3D-GS. However, Mean squared error (MSE) struggles to handle the uncertainty inherent in recovering lost high-frequency details, often leading to excessive smoothing of the rendered image. Inspired by SR-GAN [26], we add perceptual loss  $\mathcal{L}_{\text{per}}$  as a regularization term to enhance the model’s ability to perceive details. To reduce the computational overhead, we use the output of the first block before the maximum pooling of the pre-trained VGG-19:

$$\mathcal{L}_{\text{per}} = \frac{1}{CWH} \|F(G_i) - F(R_i)\|_2^2 \quad (9)$$

where  $G_i$  represents the real image,  $F(R_i)$  denotes the rendered image, and  $F$  signifies the first block of the pre-trained VGG-19 model. The dimensions of the output features are denoted by  $C$ ,  $H$ , and  $W$ .

We observe that the benefit from perceptual loss decreases with the number of iteration rounds, potentially leading to an excessive growth of Gaussians. Consequently, we reduce the weight of the perceptual loss as the number of training rounds increases. Finally,  $\mathcal{L}_{\text{per}}$  is incorporated into the loss function to obtain the total loss function as follows:

$$\mathcal{L}_{\text{Hf}} = \mathcal{L}_1 + \lambda_{\text{SSIM}} \mathcal{L}_{\text{SSIM}} + \left(1 - \frac{k}{\text{iteration}}\right) \lambda_{\text{per}} \mathcal{L}_{\text{per}} \quad (10)$$

where  $k$  denotes the current round of training and  $\text{iteration}$  denotes the total number of rounds of training.

## IV. EXPERIMENTS

### A. DataSet and Implementation

We selected eleven accessible scenarios to evaluate our method, comprising seven scenarios from Mip-NeRF360 [23] dataset, two scenarios from Tanks&Temples [27] dataset, and two scenarios from DeepBlending [28] dataset. We evaluated our method using Peak Signal-to-Noise Ratio (PSNR), Structural Similarity Index Measure (SSIM), and Learned Perceptual Image Patch Similarity (LPIPS) metrics.

In the specific implementation, the parameter settings of our model are the same as in the Scaffold-GS [2] completion,

except for our newly introduced Adaptive Frequency Encoding Module. We provide a detailed description of the parameters and complete quantitative results for each scenario in a supplementary paper.

### B. Results Analysis

In order to evaluate the effectiveness of our improvements, we choose 3D-GS [1] and Scaffold-GS [2] as the main baselines, as both methods are currently state-of-the-art. In addition, we also choose to compare with MipNeRF360 [23], iNGP [24] and Plenoxels [25], all of which have gone through 30K iterations. The results for Ours, Scaffold-GS [2], and 3D-GS [1] are obtained in our own experiments, and the rest [23]–[25] from the corresponding papers. As shown by Tab I, our method surpasses all previous methods across all datasets. The Fig. 3 compares rendering quality, featuring a green inset that zooms in on the detailed sections to better highlight the differences.

To illustrate the enhancement of our method for the ability to perceive high-frequency components, we conducted a Fourier transform on the rendered images to obtain their high-frequency component graphs. As Fig. 4 shows, AH-GS enhances the network’s ability to perceive and learn high-frequency information, resulting in rendered images that are richer in detail compared to other 3D-GS models.

### C. Ablation Studies

We present two types of experiments to measure the different contributions by gradually adding new components and altering the loss function used. Table II displays the quantitative results, and examples are shown in Fig. 5 and Fig. 6.

a) *Category 1*: Rows 3-6 are an ablation study dedicated to the Adaptive Frequency Encoding Module. We conducted experiments with two separate modules: positional encoding (pe) and density-driven frequency encoding (ddfe). These components enable the viewing direction to carry higher-frequency information, resulting in better rendering of high-frequency details.

b) *Category 2*: Rows 1-2 are an ablation study dedicated to high-frequency reinforce loss ( $\mathcal{L}_{\text{Hf}}$ ). The comparison indicates that  $\mathcal{L}_{\text{Hf}}$  enhances the performance of both Scaffold-GS to some extent. However, our method proves more effective, as it better captures the scene geometry.

TABLE I  
QUANTITATIVE RESULTS ON REAL-WORLD DATASETS.

Dataset		Mip-NeRF360			Tanks&Temples			Deep Blending		
Method	Metrics	PSNR $\uparrow$	SSIM $\uparrow$	LPIPS $\downarrow$	PSNR $\uparrow$	SSIM $\uparrow$	LPIPS $\downarrow$	PSNR $\uparrow$	SSIM $\uparrow$	LPIPS $\downarrow$
<b>Mip-NeRF360</b> [23]		29.23	0.844	0.207	22.22	0.759	0.257	29.40	0.901	0.245
<b>iNGP</b> [24]		26.43	0.725	0.339	21.72	0.723	0.330	23.62	0.797	0.423
<b>Plenoxels</b> [25]		23.62	0.670	0.443	21.08	0.719	0.379	23.06	0.795	0.510
<b>3D-GS</b> [1]		29.02	0.869	0.184	23.75	0.845	0.178	29.50	0.900	0.251
<b>Scaffold-GS</b> [2]		29.35	0.869	0.189	24.21	0.851	0.175	30.02	0.905	0.257
<b>Ours-15K</b>		29.20	0.866	0.190	23.97	0.844	0.185	29.99	0.904	0.262
<b>Ours-30K</b>		<b>29.70</b>	<b>0.871</b>	<b>0.181</b>	<b>24.42</b>	<b>0.856</b>	<b>0.168</b>	<b>30.22</b>	<b>0.906</b>	<b>0.244</b>



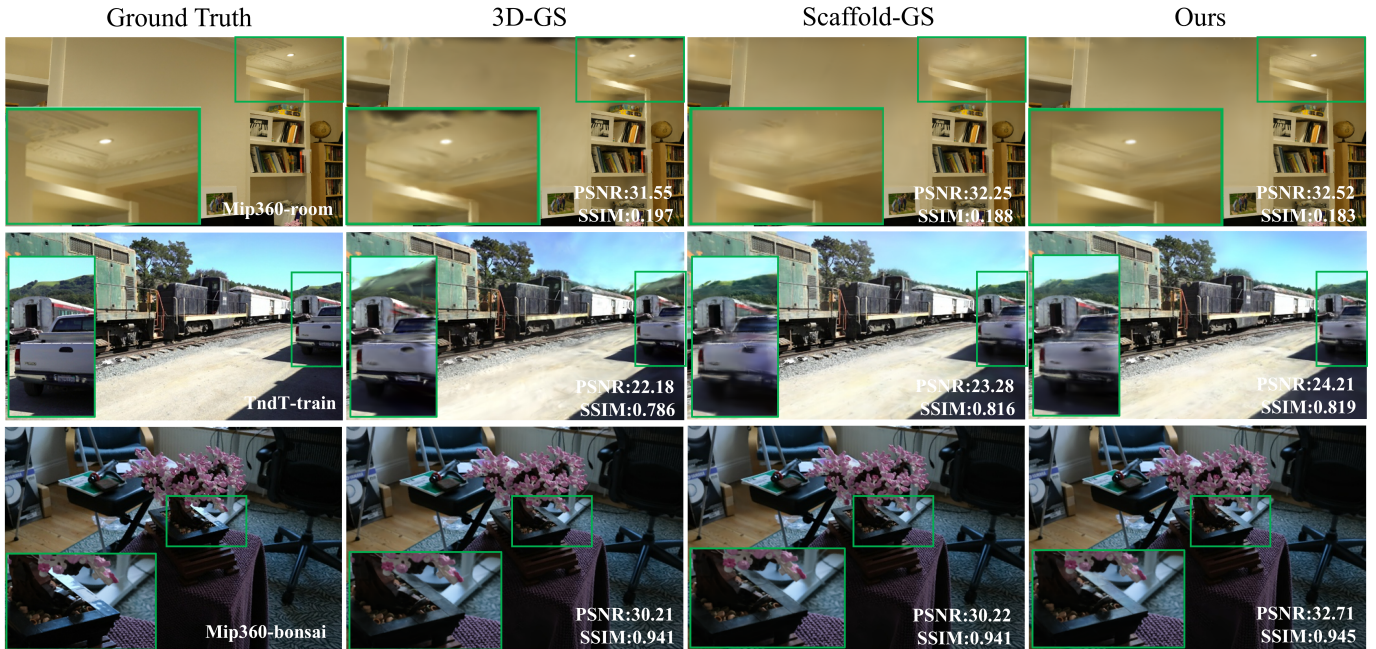


Fig. 3. Visual quality comparisons of the reconstruction results.

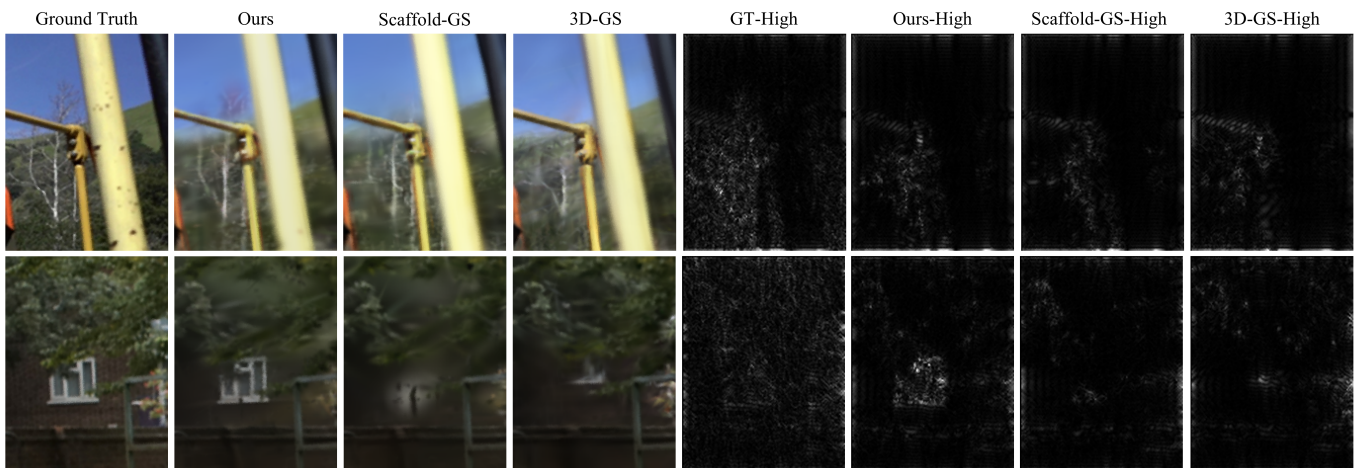


Fig. 4. Visual comparison of high-frequency details in rendered images.

TABLE II  
ABLATION STUDY ON MIPNERF360 [23] DATASET.

	PSNR $\uparrow$	SSIM $\uparrow$	LPIPS $\downarrow$
Scaffold-GS [2]	29.35	0.869	0.189
Scaffold-GS + $\mathcal{L}_{\text{HF}}$	29.49	0.873	0.180
AH-GS-full	29.70	0.871	0.181
AH-GS, No $\mathcal{L}_{\text{HF}}$	29.56	0.868	0.190
AH-GS, No $\mathcal{L}_{\text{HF}}$ , No pe	29.49	0.867	0.190
AH-GS, No $\mathcal{L}_{\text{HF}}$ , No ddfc	29.39	0.868	0.191

## V. CONCLUSION

We propose AH-GS to enhance the rendering quality of details while maintaining the real-time capabilities of 3D-GS by introducing the Adaptive Frequency Encoding Module and high-frequency reinforce loss. Extensive experiments demonstrate the effectiveness of each improvement, showing that our

approach is competitive with state-of-the-art algorithms.

## REFERENCES

- [1] Bernhard Kerbl, Georgios Kopanas, Thomas Leimkühler, and George Drettakis, “3d gaussian splatting for real-time radiance field rendering,” *ACM Transactions on Graphics*, vol. 42, no. 4, July 2023.
- [2] Tao Lu, Mulin Yu, Linning Xu, Yuanbo Xiangli, Limin Wang, Dahua Lin, and Bo Dai, “Scaffold-gs: Structured 3d gaussians for view-adaptive rendering,” in *Proceedings of the IEEE/CVF Conference on Computer Vision and Pattern Recognition*, 2024, pp. 20654–20664.
- [3] Luca De Luigi, Damiano Bolognini, Federico Domeniconi, Daniele De Gregorio, Matteo Poggi, and Luigi Di Stefano, “Scanner: a scalable benchmark for neural radiance fields,” in *Proceedings of the IEEE/CVF Winter Conference on Applications of Computer Vision*, 2023, pp. 816–825.
- [4] Muhammed Kocabas, Jen-Hao Rick Chang, James Gabriel, Oncel Tuzel, and Anurag Ranjan, “Hugs: Human gaussian splats,” in *Proceedings of the IEEE/CVF conference on computer vision and pattern recognition*, 2024, pp. 505–515.



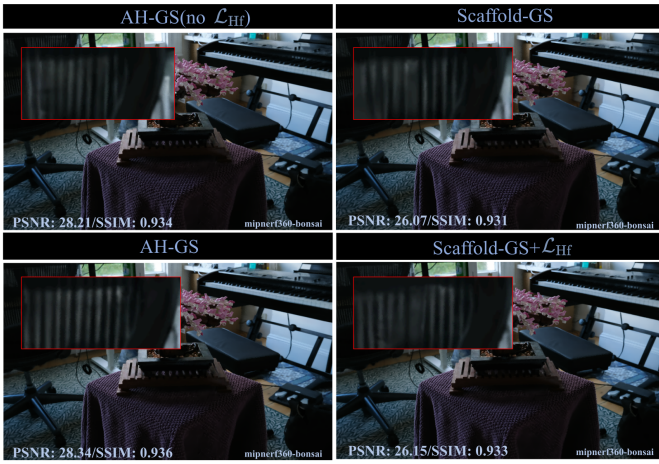


Fig. 5. Visualizing the gain of High-frequency reinforce Loss. AH-GS without high-frequency reinforce loss renders regions with little texture blurry, with a foggy crust at the edges of the image. Scaffold-GS using high-frequency reinforce loss also improves its performance to some extent and is not as good as our method in the reproduction of details.



Fig. 6. Visualizing the Gain of Adaptive Frequency Encoding Module. Removing the AFED greatly reduces the model’s ability to represent high-frequency geometries, resulting in an inability to reproduce details (e.g., windows, tree branches).

[5] Yufei Shi, Beijia Lu, Jia-Wei Liu, Ming Li, and Mike Zheng Shou, “Colonnerf: Neural radiance fields for high-fidelity long-sequence colonoscopy reconstruction,” *arXiv preprint arXiv:2312.02015*, 2023.

[6] Abril Corona-Figueroa, Jonathan Frawley, Sam Bond-Taylor, Sarath Bethapudi, Hubert PH Shum, and Chris G Willcocks, “Mednerf: Medical neural radiance fields for reconstructing 3d-aware ct-projections from a single x-ray,” in *2022 44th annual international conference of the IEEE engineering in medicine & Biology society (EMBC)*. IEEE, 2022, pp. 3843–3848.

[7] Haofan Lu, Christopher Vattheuer, Baharan Mirzasoileiman, and Omid Abari, “Newrf: A deep learning framework for wireless radiation field reconstruction and channel prediction,” in *Forty-first International Conference on Machine Learning*.

[8] Guanlin Wu, Zhonghao Lyu, Juyong Zhang, and Jie Xu, “Embracing radiance field rendering in 6g: Over-the-air training and inference with 3d contents,” *arXiv preprint arXiv:2405.12155*, 2024.

[9] Ben Mildenhall, Pratul P Srinivasan, Matthew Tancik, Jonathan T

Barron, Ravi Ramamoorthi, and Ren Ng, “Nerf: Representing scenes as neural radiance fields for view synthesis,” *Communications of the ACM*, vol. 65, no. 1, pp. 99–106, 2021.

[10] Zehao Yu, Anpei Chen, Binbin Huang, Torsten Sattler, and Andreas Geiger, “Mip-splatting: Alias-free 3d gaussian splatting,” in *Proceedings of the IEEE/CVF Conference on Computer Vision and Pattern Recognition*, 2024, pp. 19447–19456.

[11] Zhiwen Yan, Weng Fei Low, Yu Chen, and Gim Hee Lee, “Multi-scale 3d gaussian splatting for anti-aliased rendering,” in *Proceedings of the IEEE/CVF Conference on Computer Vision and Pattern Recognition*, 2024, pp. 20923–20931.

[12] Xiaowei Song, Jv Zheng, Shiran Yuan, Huan-ang Gao, Jingwei Zhao, Xiang He, Weihao Gu, and Hao Zhao, “Sa-gs: Scale-adaptive gaussian splatting for training-free anti-aliasing,” *arXiv preprint arXiv:2403.19615*, 2024.

[13] Zhiwen Fan, Kevin Wang, Kairun Wen, Zehao Zhu, Dejia Xu, and Zhangyang Wang, “Lightgaussian: Unbounded 3d gaussian compression with 15x reduction and 200+ fps,” *arXiv preprint arXiv:2311.17245*, 2023.

[14] Junli Cao, Vidit Goel, Chaoyang Wang, Anil Kag, Ju Hu, Sergei Korolev, Chenfanfu Jiang, Sergey Tulyakov, and Jian Ren, “Lightweight predictive 3d gaussian splats,” *arXiv preprint arXiv:2406.19434*, 2024.

[15] Ziyi Yang, Xinyu Gao, Wen Zhou, Shaohui Jiao, Yuqing Zhang, and Xiaogang Jin, “Deformable 3d gaussians for high-fidelity monocular dynamic scene reconstruction,” in *Proceedings of the IEEE/CVF Conference on Computer Vision and Pattern Recognition*, 2024, pp. 20331–20341.

[16] Guanjun Wu, Taoran Yi, Jiemin Fang, Lingxi Xie, Xiaopeng Zhang, Wei Wei, Wenyu Liu, Qi Tian, and Xinggang Wang, “4d gaussian splatting for real-time dynamic scene rendering,” in *Proceedings of the IEEE/CVF Conference on Computer Vision and Pattern Recognition*, 2024, pp. 20310–20320.

[17] Nasim Rahaman, Aristide Baratin, Devansh Arpit, Felix Draxler, Min Lin, Fred Hamprecht, Yoshua Bengio, and Aaron Courville, “On the spectral bias of neural networks,” in *International conference on machine learning*. PMLR, 2019, pp. 5301–5310.

[18] Preetum Nakkiran, Gal Kaplun, Dimitris Kalimeris, Tristan Yang, Benjamin L Edelman, Fred Zhang, and Boaz Barak, “Sgd on neural networks learns functions of increasing complexity,” *arXiv preprint arXiv:1905.11604*, 2019.

[19] Yuan Cao, Zhiying Fang, Yue Wu, Ding-Xuan Zhou, and Quanquan Gu, “Towards understanding the spectral bias of deep learning,” *arXiv preprint arXiv:1912.01198*, 2019.

[20] Johannes L Schonberger and Jan-Michael Frahm, “Structure-from-motion revisited,” in *Proceedings of the IEEE conference on computer vision and pattern recognition*, 2016, pp. 4104–4113.

[21] Kerui Ren, Lihan Jiang, Tao Lu, Mulin Yu, Linning Xu, Zhangkai Ni, and Bo Dai, “Octree-gs: Towards consistent real-time rendering with lod-structured 3d gaussians,” *arXiv preprint arXiv:2403.17898*, 2024.

[22] Dor Verbin, Peter Hedman, Ben Mildenhall, Todd Zickler, Jonathan T Barron, and Pratul P Srinivasan, “Ref-nerf: Structured view-dependent appearance for neural radiance fields,” in *2022 IEEE/CVF Conference on Computer Vision and Pattern Recognition (CVPR)*. IEEE, 2022, pp. 5481–5490.

[23] Jonathan T. Barron, Ben Mildenhall, Dor Verbin, Pratul P. Srinivasan, and Peter Hedman, “Mip-nerf 360: Unbounded anti-aliased neural radiance fields,” *CVPR*, 2022.

[24] Thomas Müller, Alex Evans, Christoph Schied, and Alexander Keller, “Instant neural graphics primitives with a multiresolution hash encoding,” *ACM transactions on graphics (TOG)*, vol. 41, no. 4, pp. 1–15, 2022.

[25] Sara Fridovich-Keil, Alex Yu, Matthew Tancik, Qinhong Chen, Benjamin Recht, and Angjoo Kanazawa, “Plenoxels: Radiance fields without neural networks,” in *CVPR*, 2022.

[26] Zihan Ye, Fan Lyu, Linyan Li, Qiming Fu, Jinchang Ren, and Fuyuan Hu, “Sr-gan: Semantic rectifying generative adversarial network for zero-shot learning,” in *2019 IEEE international conference on multimedia and expo (ICME)*. IEEE, 2019, pp. 85–90.

[27] Arno Knapitsch, Jaesik Park, Qian-Yi Zhou, and Vladlen Koltun, “Tanks and temples: Benchmarking large-scale scene reconstruction,” *ACM Transactions on Graphics*, vol. 36, no. 4, 2017.

[28] Peter Hedman, Julien Philip, True Price, Jan-Michael Frahm, George Drettakis, and Gabriel Brostow, “Deep blending for free-viewpoint image-based rendering,” vol. 37, no. 6, pp. 257:1–257:15, 2018.